A New Framework to Explain Changes in Io's Footprint Tail Electron Fluxes

J. R. Szalay[1] , F. Allegrini[2,3] , F. Bagenal[4] , S. J. Bolton[2] , B. Bonfond[5] , G. Clark[6] , J. E. P. Connerney[7,8] , R. W. Ebert[2,3] , V. Hue[2] , D. J. McComas[1] , J. Saur[9] , A. H. Sulaiman[10] , and R. J. Wilson[4]

[1]Department of Astrophysical Sciences, Princeton University, Princeton, NJ, USA, [2]Southwest Research Institute, San Antonio, TX, USA, [3]Department of Physics and Astronomy, University of Texas at San Antonio, San Antonio, TX, USA, [4]Laboratory for Atmospheric and Space Physics, University of Colorado Boulder, Boulder, CO, USA, [5]Space Sciences, Technologies and Astrophysics Research Institute, LPAP, Université de Liège, Liège, Belgium, [6]Johns Hopkins University Applied Physics Lab, Laurel, MD, USA, [7]Space Research Corporation, Annapolis, MD, USA, [8]Goddard Space Flight Center, Greenbelt, Maryland, USA, [9]Institute of Geophysics and Meteorology, University of Cologne, Cologne, Germany, [10]Department of Physics and Astronomy, University of Iowa, IA, USA

Abstract We analyze precipitating electron fluxes connected to 18 crossings of Io's footprint tail aurora, over altitudes of 0.15 to 1.1 Jovian radii (R_J). The strength of precipitating electron fluxes is dominantly organized by "Io-Alfvén tail distance," the angle along Io's orbit between Io and an Alfvén wave trajectory connected to the tail aurora. These fluxes best fit an exponential as a function of down-tail extent with an *e*-folding distance of 21°. The acceleration region altitude likely increases down-tail, and the majority of parallel electron acceleration sustaining the tail aurora occurs above 1 R_J in altitude. We do not find a correlation between the tail fluxes and the power of the initial Alfvén wave launched from Io. Finally, Juno has likely transited Io's Main Alfvén Wing fluxtube, observing a characteristically distinct signature with precipitating electron fluxes ~600 mW/m^2 and an acceleration region extending as low as 0.4 R_J in altitude.

Plain Language Summary The Juno spacecraft crossed magnetic field lines connected to Io's auroral signature in Jupiter's atmosphere. By measuring the electrons sustaining this auroral feature, we find that the region these electrons are accelerated is typically more than one Jovian radius away from Jupiter's atmosphere. For one of the 18 transits, we find Juno has most likely directly transited above the main auroral spot in Io's auroral signature.

1. Introduction

Jupiter's aurora is complex and dynamic, with a large number of distinct auroral features and regions generated by multiple phenomena (e.g., Grodent, 2015). Of these features, Io's auroral signature is one of the most persistent and identifiable auroras, with a rich observational history spanning decades. Remote measurements of Io's interaction with Jupiter have covered a variety of wavelengths: radio (e.g., Bigg, 1964; Dulk, 1965; Hess et al., 2009; Louis et al., 2017, 2019; Warwick et al., 1979; Zarka, 1998, 2007; Zarka et al., 2018), ultraviolet (e.g., Bonfond, Grodent, et al., 2017; Bonfond, Saur, et al., 2017; Bonfond et al., 2008, 2009, 2013; Clarke et al., 1996), infrared (e.g., Connerney et al., 1993; Mura et al., 2018; Radioti et al., 2013), and visible (e.g., Ingersoll et al., 1998).

Our understanding of Io's interaction with Jupiter's rotating magnetosphere was propelled forward after Voyager 1 flew by Io in 1979, observing magnetic and flow perturbations (Acuña et al., 1981; Belcher et al., 1981) due to an Alfvénic disturbance generated by this interaction (Goertz, 1980; Neubauer, 1980). Alfvén waves from this interaction propagate away from Io toward Jupiter's atmosphere in the northern and southern hemispheres and reflect off density gradients in the ionosphere, allowing them to bounce between hemispheres (Bagenal, 1983; Gurnett & Goertz, 1981; Hinton et al., 2019; Jacobsen et al., 2010). A consequence of this interaction is the acceleration of electrons into Jupiter's upper atmosphere, producing infrared, visible, and ultraviolet emissions associated with Io.

Io's auroral signature has four identifiable features: (1) the Main Alfvén Wing (MAW) spot (Bonfond et al., 2008; Saur et al., 2013), from Io's immediate interaction with Jupiter's corotating magnetosphere, (2)

a transhemispheric electron beam spot likely caused by conjugate electron beams from the opposite hemisphere's MAW, (3) reflected Alfvén wing spots, likely a consequence of Alfvén wave reflections across density gradients in the Io torus, and (4) a long auroral tail.

Before the Juno mission (Bolton et al., 2017), two separate mechanisms had been proposed to explain Io's auroral tail. One mechanism involves a quasi-steady current system transferring angular momentum to subcorotational plasma in Io's wake (e.g., Delamere et al., 2003; Ergun et al., 2009; Hill & Vasyliunas, 2002; Matsuda et al., 2012; Su et al., 2003). This setup, with large quasi-static parallel potential structures that accelerate electrons toward Jupiter, would be observable via peaked electron intensities ~1–70 keV. The other proposed mechanism involves a system of Alfvén waves sustained by multiple reflections down-tail which bidirectionally accelerate electrons each successive bounce (e.g., Bonfond, Saur, et al., 2017; Bonfond et al., 2009; Crary & Bagenal, 1997; Hess et al., 2010, 2013; Jacobsen et al., 2007, 2010) and would observationally exhibit broad electron intensity spectra and bidirectional fluxes within the acceleration region.

Since Juno arrived at Jupiter, its diverse set of instruments have revealed an even more complex and dynamic picture of Io's auroral interaction, having made close-in Io tail observations of infrared emissions (Mura et al., 2018), UV emissions (Bonfond, Gladstone, et al., 2017; Hue et al., 2019; Szalay et al., 2018), electrons and ions (Szalay et al., 2018, 2020), energetic particle dropouts (Paranicas et al., 2019), wave-particle interactions (Sulaiman et al., 2020), ion conics (Clark et al. 2020), and Alfvénic turbulence (Gershman et al., 2019). To date, these measurements favor an Alfvénic acceleration mechanism sustaining tail emissions (Damiano et al., 2019; Gershman et al., 2019; Saur et al., 2018; Sulaiman et al., 2020; Szalay et al., 2018; Szalay, Bagenal, et al., 2020). Io's intense interaction allows us to probe the physics of moon-magnetosphere interactions, and the results can be applicable to analogous interactions at other planets, such as the Enceladus-related auroral emissions at Saturn (e.g., Pryor et al., 2011; Sulaiman et al., 2018) and Triton at Neptune.

After nearly 4 years in orbit, Juno has transited flux tubes connected to Io's footprint tail aurora dozens of times. Here, we focus on 18 identifiable tail encounters, providing a sufficient spread in parameter space to allow for a statistically meaningful study of the Io tail precipitating electron fluxes. In section 2, we discuss the measurements used in this analysis. In section 3, we discuss the specifics of how to measure "down-tail extent" and present a new trend for the fluxes sustaining the footprint tail aurora. We conclude in section 4 with a discussion of these results.

2. In Situ Measurements

Electron observations are obtained by the Jovian Auroral Distributions Experiment, JADE (McComas et al., 2017). JADE consists of two electron sensors (JADE-E) capable of measuring electrons in the energy range of 50 eV to 100 keV and one ion sensor (JADE-I). Previous measurements from JADE allowed for estimations of various auroral regions by identifying specific features in both the JADE electron and ion fluxes (e.g., Allegrini et al., 2017, 2020; Ebert et al., 2017, 2019; Szalay et al., 2017; Valek et al., 2019); Io's tail signatures are one of the most persistently identifiable features.

To relate high-latitude measurements to the equatorial region, we use the JRM09 internal magnetic field (Connerney et al., 2018) in combination with a magnetodisc model (Connerney et al., 1981) to trace magnetic field lines from the Juno spacecraft's position to the equator; this determines "M shell," distinct from the strictly dipolar "L shell." Mapping the field to the ionosphere establishes Juno's magnetic footprint. For each Juno perijove (PJ), we manually identify when Juno magnetically maps to the Io torus inner boundary M shells just interior to 6 R_J. This boundary is readily identifiable in the JADE ion data as a sharp cutoff in ion flux (e.g., Szalay et al., 2017; Valek et al., 2019). Io footprint tail crossings occur just further than the M shell of this boundary and are particularly prominent in this region, which typically has very low fluxes of electrons above 50 eV. While Juno may cross flux tubes connected to Io's footprint tail more than twice per perijove, we only consider crossings during Juno's very near approach within altitudes of <1.1 Jovian radii (R_J), measured from the surface of an oblate ellipsoid with axes of 71,492 and 66,854 km. This altitude restriction ensures that JADE-E can resolve the loss cone, as farther crossings occur when JADE-E often cannot electrostatically deflect to measure field-aligned electrons or the loss cone is smaller than JADE-E's angular resolution of ~7.5°. We have also applied a new method to enhance the time resolution of

JADE-E data (Text S1 in the supporting information) and additional background subtraction over the nominal JADE-E methods (Text S2 in the supporting information) due to enhanced radiation encountered when magnetically connected to Io's orbital distance (e.g., Nénon et al., 2018).

Figure 1 shows four examples of tail crossings during perijoves 5 South, 12 North, 14 North, and 22 North. Panels (a) and (c) show the upward and downward differential energy flux (DEF). Panel (b) shows the DEF pitch angle (PA) distribution, where downward pitch angles are at the bottom and upward at the top, hence northern hemisphere PA panels run from 180° to 0° and southern hemisphere PA panels from 0° to 180° in pitch angle. Panel (d) shows the downward precipitating energy flux in the loss cone for nominal (gray crosses) and Io tail specific (black circles) background subtraction schemes. Pitch angles are calculated using the broadcast magnetic field vector from the MAG instrument (Connerney et al., 2017). Energy flux is calculated as $EF = \pi \sum_i DEF_i \cdot \Delta E_i$, where the sum (subscript i) occurs over JADE-E energy steps, π is the area-projection weighted size of the loss cone above Jupiter's atmosphere, and ΔE_i is the width of each energy bin (e.g., Mauk et al., 2017). Gray regions indicate where JADE-E did not make measurements.

Panel (e) shows the differential number flux (DNF) as a function of energy (intensity spectra). Spectra are colored as a function of time corresponding to the horizontal color strip at the top above subpanel (a). Gray spectra correspond to time ranges under the gray bars in the color strip. All quantities with the exception of the gray crosses in panel (d) are shown with nominal plus Io tail specific background subtraction (Text S2 in the supporting information). While the additional background subtraction method is able to successfully isolate the Io footprint tail signal, we do not show error bars given the difficulty in quantifying these for the background scheme used here (Text S2 in the supporting information).

Up to and including PJ26, we identified 18 Io footprint tail crossings during close approach (Table S1 in the supporting information). For each crossing, we calculate the peak energy flux (EF) after all backgrounds are subtracted. Note, this additional background subtraction leads to lower derived energy fluxes than previously calculated (Szalay et al., 2018). The four examples shown in Figure 1 highlight many of the types of features observed during these crossings. While Juno transited flux tubes for down-tail angles $\Delta\lambda_{\text{Alfvén}} \geq 135°$ (defined in the next section), we were either unable to detect an appreciable signal, or unable to reasonably calculate the energy flux given instrumental backgrounds. All tail crossings exhibited broad, power law-like intensity distributions, indicative of broadband acceleration as previously reported for Io footprint tail crossings (Szalay et al., 2018).

PJ5S exhibits a bifurcated feature in upward fluxes, but we are unable to resolve if this feature existed in downward fluxes due to the pitch angle coverage gap. PJ12N represents the largest fluxes observed by JADE for a tail transit at 580 mW/m². Unlike the large majority of transits, JADE observed nearly equal upward and downward electron fluxes. Bidirectional electron fluxes are predicted to exist within the Alfvénic acceleration region due to field-aligned, oscillating electric fields (Hess et al., 2010; Jones & Su, 2008), hence, this indicates that Juno may have been immersed in the electron acceleration zone at its altitude of 0.4 R_J. PJ14N exhibited multiple distinct flux features separated by dropouts, indicative of a complex tail structure. PJ22N registered the second largest downward energy fluxes and had two unique features mapping to the Jupiter-ward edge of the crossing: (1) an upward electron conic at the end of the primary feature and (2) primarily upward discrete electron fluxes, with inverted-V structure. While these four crossings show much of the character of fluxes JADE observed, all 18 crossings are individually shown in the same format in the supporting information.

3. Trend as a Function of Down-Tail Extent

To cross-compare tail crossings, we need a metric for how far down-tail each occurred. We consider three metrics, summarized in the top row of Figure 2: $\Delta\lambda_{\text{Lon}}$ = difference in Sys. III longitude between the MAW and Juno footprint; $\Delta\lambda_{\text{Frac}}$ = fractional distance along the statistical Io footprint track between the MAW and Juno footprint; and $\Delta\lambda_{\text{Alfvén}}$ = the angular separation along Io's orbit between Io and an Alfvén wave trajectory back-traced from Juno's footprint.

$\Delta\lambda_{\text{Lon}}$ is the simplest to calculate, requiring only the System III longitudes of the MAW (Bonfond, Saur, et al., 2017) and Juno's magnetically mapped footprint. However, a simple difference in System III longitude does not provide a consistent metric since the extent varies as a function of the location of the MAW. For example,
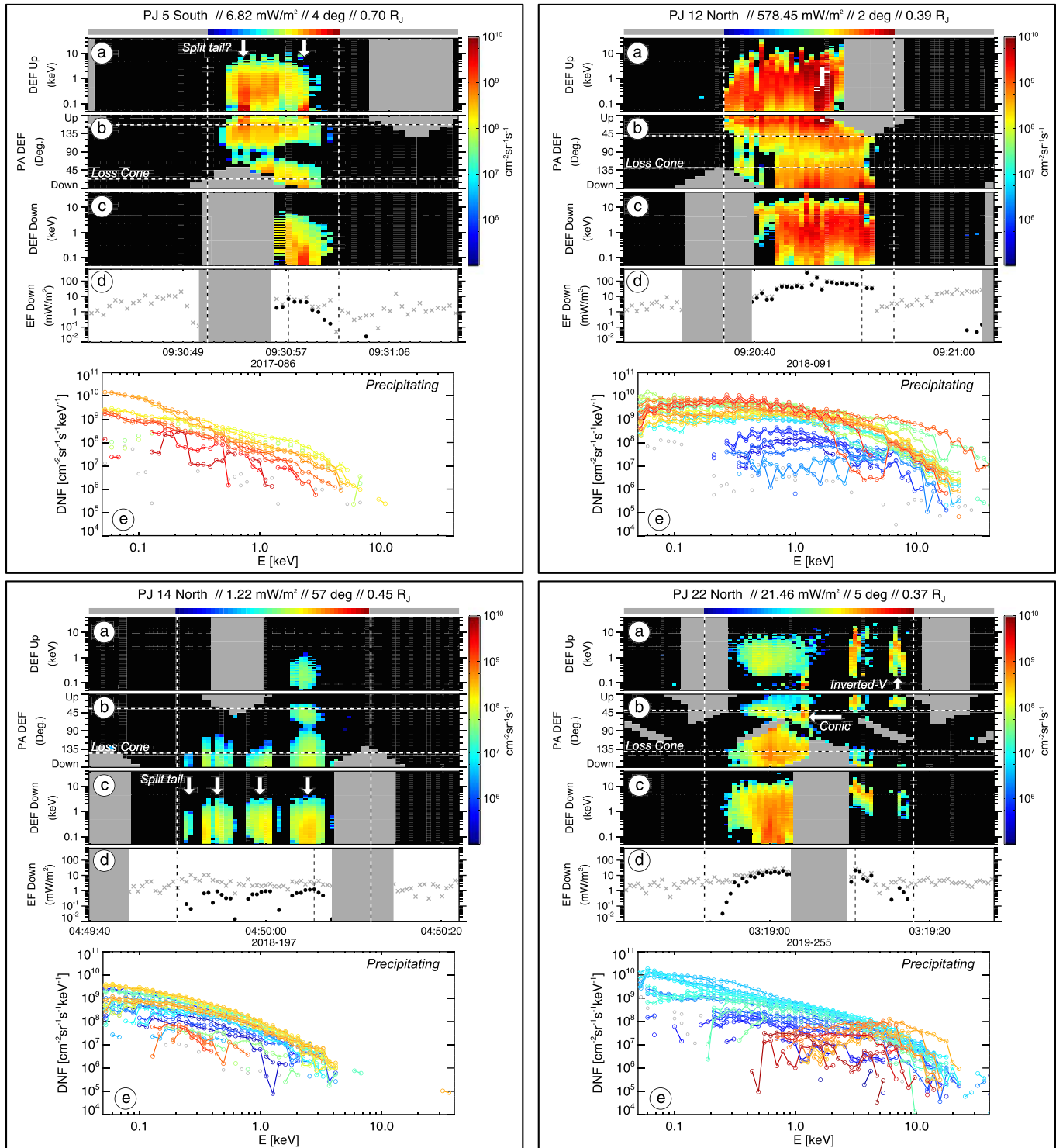
Figure 1. Spectrograms for four tail transits: PJ5S, PJ12N, PJ14N, PJ22N. All spectrograms are in differential energy flux (DEF). Subpanels (a) and (c) show DEF within the upward and downward loss cone, subpanel (b) shows the pitch angle distribution, subpanel (d) shows the total precipitating energy fluxes before (gray crosses) and after (black circles) Io-specific background subtraction, and subpanel (e) shows the intensity as a function of energy within the downward loss cone (precipitating). The spectra are color coded by the time in the horizontal color strip at the top of (a). Text at the top shows PJ, EF_{peak}, $\Delta\lambda_{Alfvén}$, and altitude.
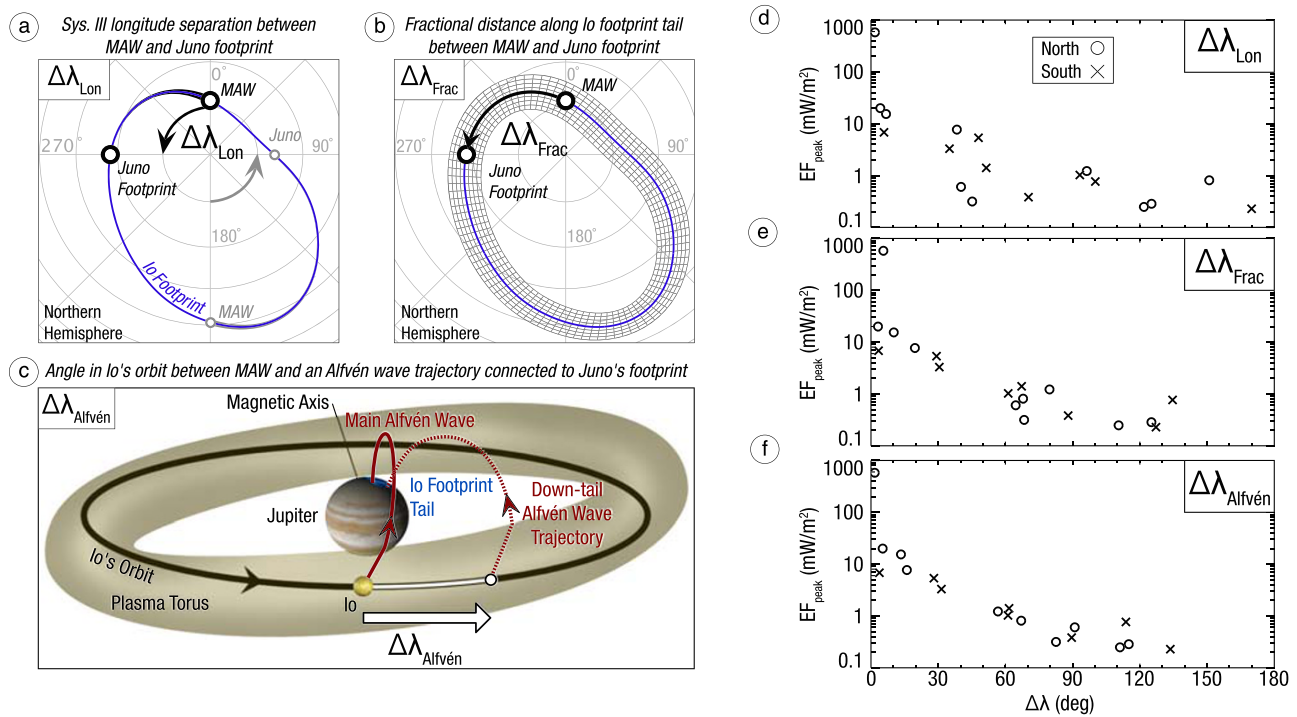
Figure 2. Three measures of down-tail extent investigated in this work. (a) Difference in system III longitude between the Main Alfvén wing (MAW) and Juno's magnetic footprint. (b) Fractional distance along the statistical Io footprint track between the MAW and Juno's footprint. (c) Angular separation along Io's orbit between Io and an Alfvén wave trajectory connected to Juno's footprint (adapted from Saur et al., 2004). Panels (d)–(f) show energy flux as a function angle for each down-tail metric.

both pairs of MAW/Juno footprints shown in black and gray in Figure 2a are separated by 90° in System III longitude and would therefore correspond to an angular separation of $\Delta\lambda_{\text{Lon}} = 90°$. However, the gray example covers approximately twice the arclength along Io's statistical footprint track as the example shown in black.

$\Delta\lambda_{\text{Frac}}$ attempts to correct this inconsistency by using the fractional arclength along the Io footprint track as a measure of down-tail extent. To do so, we set up a coordinate system with one axis parallel to the Io footprint track, shown with the gray grid in Figure 2b. We then calculate the total down-tail distance between the MAW and Juno footprint parallel to the Io footprint track and normalize it by the total arclength of the Io footprint track, which is 198,360 km in the northern hemisphere and 188,180 km in the southern hemisphere (Bonfond, Saur, et al., 2017). $\Delta\lambda_{\text{Frac}}$ is calculated by multiplying this fraction by 360°, more accurately accounting for the fact that total arclength separations vary as a function System III longitude. Yet this metric assumes each unit length along the Io footprint track corresponds to the same change in down-tail extent.

Both $\Delta\lambda_{\text{Lon}}$ and $\Delta\lambda_{\text{Frac}}$ compare the instantaneous position of Juno's magnetic footprint with Io's Main Alfvén Wing. In some ways, this is an inconsistent comparison, as the MAW is the location on Jupiter's atmosphere that an Alfvén wave trajectory ends when launched from Io's instantaneous position. The Juno footprint, on the other hand, is the magnetically (not Alfvénically) mapped location of Juno on Jupiter's atmosphere. Therefore, both metrics cross-mix Alfvén wave trajectories with magnetic field mappings. $\Delta\lambda_{\text{Alfvén}}$, the "Io-Alfvén tail distance", represents a more physically robust metric by tracing an Alfvén wave from Juno's magnetic footprint at Jupiter back to its origin in Io's orbital plane. To do so, we must estimate the average path that an Alfvén wave would take from Io's orbital plane to Jupiter's atmosphere.

Previous UV observations with HST give the location of the MAW as a function of Io's location in its orbit (Bonfond, Saur, et al., 2017). This relation (via a Fourier fit of HST observations) gives the location on Jupiter's surface magnetically connected to the electron acceleration region, which is subsequently connected to Io via an Alfvén wave. While this mapping could also be performed via a modeling construct
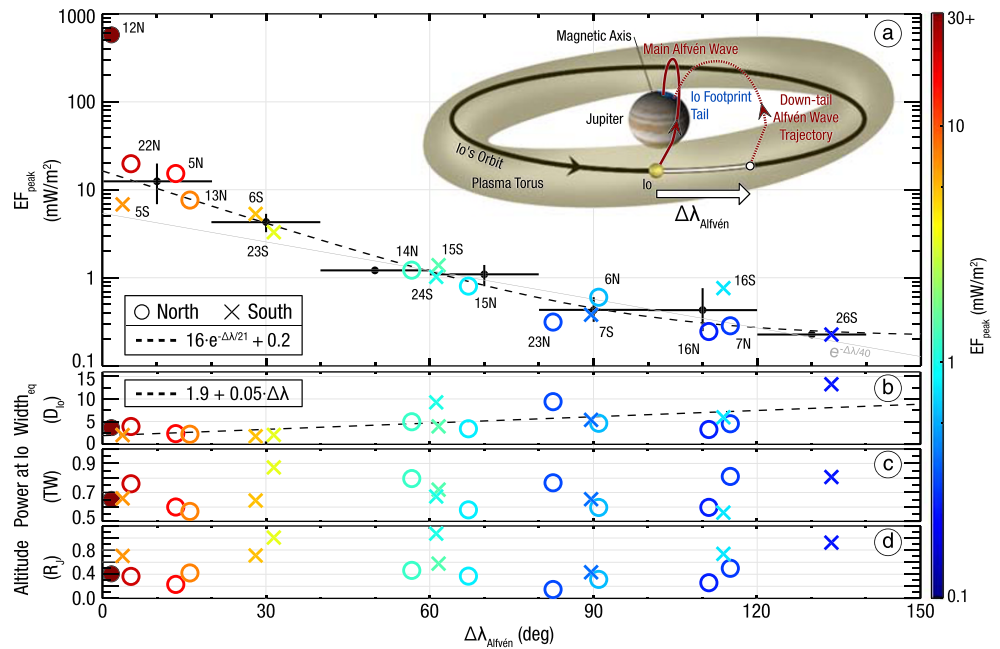
Figure 3. (a) Peak energy flux, (b) equatorial width, (c) power generated at Io, and (d) Juno altitude from a reference ellipsoid as a function of $\Delta\lambda_{Alfvén}$ for each Io footprint tail crossing. All points are color coded by energy flux. Dashed lines show least squares fits of (a) an exponential function to the data in 20° bins and (b) a linear fit to all data. PJ12N shown with the filled red circle is excluded from the binning and fits.

(e.g., Hinton et al., 2019), we implement the empirical fit to back-trace Alfvén waves from Juno's magnetic footprint to their previous position along Io's orbit. This is perhaps the most physically consistent metric to compare down-tail distance, given that the MAW physically corresponds to tracing an Alfvén wave trajectory from Io to the Jovian atmosphere and we are now comparing an angle within an orbit consistently between two Alfvén waves.

The right column of Figure 2 shows how the peak electron energy fluxes are organized as a function tail angle, also given in Table S1 in the supporting information. $\Delta\lambda_{Lon}$, the most basic and least consistent method, provides a rough organization to the data (Figure 2d), generally exhibiting decreasing fluxes as a function of angle. However, there is significant scatter in this trend. $\Delta\lambda_{Frac}$ provides a tighter trend, yet there is still a fair amount of spread in the data (Figure 2e). The largest flux observed (the top circle at $580\,\mathrm{mW/m^2}$) occurs at $\Delta\lambda_{Frac} = 6°$ and does not fit well into the trend. $\Delta\lambda_{Alfvén}$ provides the best organization and tightest trend to the data (Figure 2f). The largest observed flux occurs at $\Delta\lambda_{Alfvén} = 1.7°$, and the spread in the data is the smallest of the three methods. Given the low spread, coherent trend, and that comparing Alfvén wave mappings is the most physically consistent way to compare down-tail extent, we favor the Io-Alfvén tail distance $\Delta\lambda_{Alfvén}$ in this work.

Figure 3 shows all 18 crossings as a function $\Delta\lambda_{Alfvén}$ for (a) peak energy flux, (b) width of the feature mapped to Io's orbital plane with the JRM09 model, (c) power generated by Io (Hess et al., 2010) accounting for the Alfvén travel time (Text S3 in the supporting information), and (d) Juno's altitude. The power values shown in Figure 3c are modeled by estimating local magnetic field and induced current across Io due to its interaction with Jupiter's rotating magnetosphere (Hess et al., 2010). Each perijove (PJ) is labeled, where circles and crosses correspond to northern and southern crossings respectively. To account for variations in fluxes at similar angles and for the data spanning multiple decades, we bin the fluxes into 20° bins and fit to these binned fluxes using a nonlinear least squares fit (Markwardt, 2009). We use the range of values in each bin for errors in the fit. For bins with only one flux, we assume an error of 50% of that value.

The dashed line in Figure 3a shows an exponential with a small offset, $EF = 16 \cdot e^{-\Delta\lambda_{Alfvén}/21°} + 0.2\,\mathrm{mW/m^2}$. The PJ12N flux is excluded from the binning and fit as an outlier, due to the likelihood Juno transited the

MAW during this time (discussed in the next section). An exponential decay has been used both theoretically and observationally, (e.g., Bonfond, Saur, et al., 2017 and references therein) to describe the UV tail emissions as a function of down-tail extent, where the previous observationally derived e-folding value of 40° is shown with the gray line in Figure 3a. To better match the data, we included a vertical offset, indicating that additional backgrounds may exist at ~0.2 mW/m^2.

Figure 3b shows that the equatorial width of the Io tail feature broadens as function of $\Delta\lambda_{Alfvén}$, where the dashed line shows a linear fit to all data points with equal weighting (excluding PJ12N). Figures 3c and 3d show additional quantities that could potentially affect the observed energy flux; however, we do not find any strong correlations in energy flux with the available energy at Io's original position (Figure 3c) nor with Juno's altitude (Figure 3d). For example, as shown in Figure 3c, PJ23S corresponds to an initial Io generated power of ~50% more than PJ6S, yet, PJ23S's energy flux is a factor of ~2 less than PJ6S's. With the altitude dependence, for example, PJ7N, PJ16N, and PJ16S occur at nearly identical tail separations, but are taken over an altitude range of 0.26 to 0.74 R_J. If the electron acceleration region was within this altitude range, we would expect the lower-altitude observations to show larger downward precipitating electron flux; however, the opposite trend is true. There are many other groupings where there is no clear dependence on altitude or Io's position in the torus.

4. Discussion and Conclusions

We identify 18 distinct Io footprint tail transits in the Juno data and calculate the peak precipitating energy flux for each. The tail crossing energy fluxes exhibit a well-organized trend as a function of down-tail extent following an exponential with an *e*-folding distance of 21°. This value is consistent with theoretical estimates of the *e*-folding distance ~20°. It is a factor of 2 lower than the previous observational value of ~40° derived from Hubble Space Telescope limb observations (Bonfond et al., 2008; Bonfond, Saur, et al., 2017). However, the HST observations occurred for angular separations <55° and used a definition of down-tail extent similar to $\Delta\lambda_{Frac}$, that is, the down-tail arc-length along Io's footprint tail. As shown in Figure 2, the definition of down-tail extent affects the interpretation of these fluxes. The difference between the two observational values may be due to differing down-tail metrics and the different angular ranges explored. We favor the physically motivated down-tail definition outlined in this work of the "Io-Alfvén tail distance", $\Delta\lambda_{Alfvén}$: the angle in Io's orbit between an Alfvén wave trajectory connected to the Io footprint tail and Io itself.

Six of the crossings exhibited split tails (one or multiple dropouts in the precipitating electron fluxes) as previously discussed in the literature (Szalay et al., 2018) and indicated in Table S1. Some, like PJ14N, had more than two distinguishable "split" flux features. Transits with split features occurred for $\Delta\lambda_{Alfvén} = 4°$ to 114° and all but the PJ14N split tails occurred for southern hemispheres. However, other perijoves may also have split features that cannot be detangled from pitch angle coverage gaps. The split features may be related to the observed widening of the tail (Figure 3b). We also note the fitted width of the tail near the MAW of 1.9 D_{Io} is smaller, yet similar to the width of 2.7 D_{Io} determined for accelerated proton structures observed during a PJ18 tail crossing (Szalay, Bagenal, et al., 2020) that may have been connected to the MAW, occurring at $\Delta\lambda_{Alfvén} = 1.6°$ to 1.8°.

Additionally, PJ6N (91°, Figure S6N in the supporting information) and PJ22N (5°, Figure 1) exhibited upward electron fluxes within the loss cone mapping Jupiter-ward of Io's orbit, along with electron conics, similar to those observed during Juno's transit of Ganymede's footprint tail (Szalay et al., 2020). PJ22N also exhibited upward inverted-V's, which could be related to return currents and/or signatures of low-energy potential jumps in radio emissions associated with the Io footprint (Hess et al., 2009).

All crossings exhibited broad, power-law-like intensity distributions. Without comparing to coincident magnetic field data, we cannot conclusively determine whether these signatures are Alfvénically accelerated versus another broadband acceleration mechanism. Yet, given the success of the Alfvén wave back-tracing and that the distributions are not consistent with static downward inverted-V acceleration, such distributions fit within the body of increasing evidence for Alfvénic acceleration sustaining tail emissions in the Juno era (Bonfond, Saur, et al., 2017; Damiano et al., 2019; Gershman et al., 2019; Saur et al., 2018; Sulaiman

et al., 2020; Szalay, Bagenal, et al., 2020; Szalay et al., 2018). We mention that during the PJ12N transit, Poynting fluxes associated with the turbulent cascade of low-frequency transverse fluctuations in the magnetic field indicative of Alfvénic fluctuations were estimated to be ~3,000 mW/m^2 (Gershman et al., 2019). The contemporaneous field and particle measurements suggest that magnetic field turbulence is a likely mechanism for the energization of electron fluxes ~600 mW/m^2 (Gershman et al., 2019; Sulaiman et al., 2020).

The tail fluxes do not encode the strength of the initial Alfvén wave power, evidenced by a lack of correlation between Io-generated power and precipitating electron flux. We note that the efficiency of electron energization due to Alfvén waves is dependent on the perpendicular length scale and unperturbed electron density and temperature (e.g., Lysak & Lotko, 1996; Saur et al., 2018; Watt & Rankin, 2007, 2012). The correlation with initial Alfvén power, which itself has inherint variability (e.g., Blöcker et al., 2020), could be obscured if these quantities have additional variability down-tail. The lack of strong altitude dependence and depleted upward loss cones suggest the majority of electron acceleration is occurring above an altitude of 1.1 R_J. This is consistent with previous Alfvénic acceleration models, where much of the expected acceleration occurs above the peak in parallel electric field, estimated to occur around 1 R_J altitude (e.g., Hess et al., 2010; Jones & Su, 2008). However, the two crossings nearest to the MAW (PJ5S and PJ12N) exhibited similar amounts of upward vs. downward loss cone fluxes, suggesting Juno transited the acceleration region (e.g., Hess et al., 2010; Jones & Su, 2008) at altitudes of 0.4–0.7 R_J within $\Delta\lambda_{\text{Alfvén}} \leq 4°$ and that this region increases in altitude down-tail.

JADE observed fluxes are consistent with previous HST derived values. Within 60°, previous (non-MAW) tail precipitating energy fluxes were estimated to range from 2–20 mW/m^2 (Bonfond et al., 2009). The Juno in situ measurements presented here have fluxes of 1–20 mW/m^2 within 60° of the MAW, excluding the PJ12N transit. Given how close the PJ12N transit Alfvénically maps to Io ($\Delta\lambda_{\text{Alfvén}} = 1.5°$–1.8° across the transit) and its location on the trend with fluxes ~600 mW/m^2, within the range of previous MAW estimates of 250–2,000 mW/m^2 (Bonfond et al., 2013), we suggest Juno probably directly transited the MAW at this time. This is further bolstered by the fact that the MAW and first torus-reflected Alfvén wing emissions are coincident during this transit, such that the MAW spot should have significantly enhanced emissions compared to its near-tail emissions.

The difference between PJ12N ($\Delta\lambda_{\text{Alfvén}} = 2°$) and PJ5S ($\Delta\lambda_{\text{Alfvén}} = 4°$) provides an interesting comparison, as Juno observed a factor of 85 lower fluxes during PJ5S. These observations occurred for nearly identical initial Io powers (Figure 3c) and torus configurations. For both, Io was near the opposite hemisphere's torus boundary such that the MAW and first torus-reflected Alfvén wave nearly coincide (Bonfond et al., 2008). The PJ5S fluxes were lower than the next three farther transits, out to 16°. Recent high-resolution infrared images have shown considerable substructure immediately down-tail of the MAW (Mura et al., 2018). We suggest that for PJ5S, Juno transited field lines nearly connected to an emission gap in Io's tail emissions, which occurs for similar angular separations (where 4° corresponds to ~2,100 km down-tail in Jupiter's atmosphere).

The main conclusions for this work are summarized below.

1. Electron energy fluxes are best organized by the "Io-Alfvén tail distance": The angular separation along Io's orbit between Io and an Alfvén wave trajectory back-traced from Jupiter's ionosphere;
2. electron energy fluxes diminish following an exponential in the tail direction with an *e*-folding distance of 21°;
3. the width of the tail increases as a function of down-tail extent;
4. electron fluxes in the tail do not correlate with the initial power of the Alfvén wave launched from Io;
5. the acceleration region altitude likely increases down-tail, where the majority of parallel electron acceleration sustaining the tail aurora occurs above 1 R_J in altitude;
6. for a few transits, the Io footprint tail exhibited upward electron conics, similar to Ganymede's footprint tail; and
7. Juno has likely directly crossed Io's Main Alfvén Wing spot in the northern portion of perijove 12, observing a characteristically distinct signature with intense precipitating electron fluxes ~600 mW/m^2 and an acceleration region extending as low as 0.4 R_J in altitude.

Data Availability Statement

The JNO-J/SW-JAD-3-CALIBRATED-V1.0 JADE-E Version 03 files were obtained from the Planetary Data System (PDS) at this site (https://pds.nasa.gov/).

References

Acuña, M. H., Neubauer, F. M., & Ness, N. F. (1981). Standing Alfvén wave current system at Io: Voyager 1 observations. *Journal of Geophysical Research*, *86*(A10), 8513–8521. https://doi.org/10.1029/JA086ia10p08513

Allegrini, F., Bagenal, F., Bolton, S., Connerney, J., Clark, G., Ebert, R. W., et al. (2017). Electron beams and loss cones in the auroral regions of Jupiter. *Geophysical Research Letters*, *44*, 1–9. https://doi.org/10.1002/2017GL073180

Allegrini, F., Mauk, B. H., Clark, G., Gladstone, G. R., Hue, V., Kurth, W. S., et al. (2020). Energy flux and characteristic energy of electrons over Jupiter's main auroral emission. *Journal of Geophysical Research: Space Physics*, *125*, 1–25. https://doi.org/10.1029/2019JA027693

Bagenal, F. (1983). Alfvén wave propagation in the Io plasma torus. *Journal of Geophysical Research*, *88*(A4), 3013. https://doi.org/10.1029/JA088ia04p03013

Belcher, J. W., Goertz, C. K., Sullivan, J. D., & Acuña, M. H. (1981). Plasma observations of the Alfvén wave generated by Io. *Journal of Geophysical Research*, *86*(A10), 8508–8512. https://doi.org/10.1029/JA086ia10p08508

Bigg, E. K. (1964). Influence of the satellite Io on Jupiter's decametric emission. *Nature*, *203*(4949), 1008–1010. https://doi.org/10.1038/2031008a0

Blöcker, A., Roth, L., Ivchenko, N., & Hue, V. (2020). Variability of Io's poynting flux: A parameter study using MHD simulations. *Planetary and Space Science*, *192*, 105058. https://doi.org/10.1016/j.pss.2020.105058

Bolton, S. J., Lunine, J., Stevenson, D., Connerney, J. E. P., Levin, S., Owen, T. C., et al. (2017). The Juno mission. *Space Science Reviews*, *213*(1–4), 5–37. https://doi.org/10.1007/s11214-017-0429-6

Bonfond, B., Gladstone, G. R., Grodent, D., Greathouse, T. K., Versteeg, M. H., Hue, V., et al. (2017). Morphology of the UV aurorae Jupiter during Juno's first perijove observations. *Geophysical Research Letters*, *44*, 4463–4471. https://doi.org/10.1002/2017GL073114

Bonfond, B., Grodent, D., Badman, S. V., Saur, J., Gérard, J.-C., & Radioti, A. (2017). Similarity of the Jovian satellite footprints: Spots multiplicity and dynamics. *Icarus*, *292*, 208–217. https://doi.org/10.1016/j.icarus.2017.01.009

Bonfond, B., Grodent, D., Gérard, J.-C., Radioti, A., Dols, V., Delamere, P. A., & Clarke, J. T. (2009). The Io UV footprint: Location, inter-spot distances and tail vertical extent. *Journal of Geophysical Research*, *114*, A07224. https://doi.org/10.1029/2009JA014312

Bonfond, B., Grodent, D., Gérard, J.-C., Radioti, A., Saur, J., & Jacobsen, S. (2008). UV Io footprint leading spot: A key feature for understanding the UV Io footprint multiplicity? *Geophysical Research Letters*, *35*, L05107. https://doi.org/10.1029/2007GL032418

Bonfond, B., Hess, S. L. G., Bagenal, F., Gérard, J.-C., Grodent, D., Radioti, A., et al. (2013). The multiple spots of the Ganymede auroral footprint. *Geophysical Research Letters*, *40*, 4977–4981. https://doi.org/10.1002/grl.50989

Bonfond, B., Saur, J., Grodent, D., Badman, S. V., Bisikalo, D., Shematovich, V., et al. (2017). The tails of the satellite auroral footprints at Jupiter. *Journal of Geophysical Research: Space Physics*, *122*, 7985–7996. https://doi.org/10.1002/2017JA024370

Clark, G., Kollmann, P., Saur, J., Mauk, B. H., Paranicas, C., Allegrini, F., et al. (2020). Energetic proton acceleration associated with Io's footprint tail. *Geophysical Research Letters*.

Clarke, J. T., Ballester, G. E., Trauger, J., Evans, R., Connerney, J. E. P., Stapelfeldt, K., et al. (1996). Far-ultraviolet imaging of Jupiter's Aurora and the Io "Footprint". *Science*, *274*(5286), 404–409. https://doi.org/10.1126/science.274.5286.404

Connerney, J. E. P., Açuna, M. H., & Ness, N. F. (1981). Modeling the Jovian current sheet and inner magnetosphere. *Journal of Geophysical Research*, *86*(A10), 8370–8384. https://doi.org/10.1029/JA086ia10p08370

Connerney, J. E. P., Baron, R., Satoh, T., & Owen, T. (1993). Images of excited H_3^+ at the foot of the Io flux tube in Jupiter's atmosphere. *Science*, *262*(5136), 1035–1038. https://doi.org/10.1126/science.262.5136.1035

Connerney, J. E. P., Benn, M., Bjarno, J. B., Denver, T., Espley, J., Jorgensen, J. L., et al. (2017). The Juno magnetic field investigation. *Space Science Reviews*, *213*(1–4), 39–138. https://doi.org/10.1007/s11214-017-0334-z

Connerney, J. E. P., Kotsiaros, S., Oliversen, R. J., Espley, J. R., Joergensen, J. L., Joergensen, P. S., et al. (2018). A new model of Jupiter's magnetic field from Juno's first nine orbits. *Geophysical Research Letters*, *45*, 2590–2596. https://doi.org/10.1002/2018GL077312

Crary, F. J., & Bagenal, F. (1997). Coupling the plasma interaction at Io to Jupiter. *Geophysical Research Letters*, *24*(17), 2135–2138. https://doi.org/10.1029/97GL02248

Damiano, P. A., Delamere, P. A., Staffer, B., Ng, C.-S., & Johnson, J. R. (2019). Kinetic simulations of electron acceleration by dispersive scale Alfvén waves in Jupiter's magnetosphere. *Geophysical Research Letters*, *46*, 3043–3051. https://doi.org/10.1029/2018GL081219

Delamere, P. A., Bagenal, F., Ergun, R. E., & Su, Y. J. (2003). Momentum transfer between the Io plasma wake and Jupiter's ionosphere. *Journal of Geophysical Research*, *108*(A6), 1241. https://doi.org/10.1029/2002JA009530

Dulk, G. A. (1965). Related Radio Emission from Jupiter. *Science*, *148*. https://doi.org/10.1126/science.148.3677.1585

Ebert, R. W., Allegrini, F., Bagenal, F., Bolton, S. J., Connerney, J. E. P., Clark, G., et al. (2017). Spatial distribution and properties of 0.1-100 keV electrons in Jupiter's polar Auroral region. *Geophysical Research Letters*, *44*, 9199–9207. https://doi.org/10.1002/2017GL075106

Ebert, R. W., Greathouse, T. K., Clark, G., Allegrini, F., Bagenal, F., Bolton, S. J., et al. (2019). Comparing Electron energetics and UV brightness in Jupiter's northern polar region during Juno Perijove 5. *Geophysical Research Letters*, *46*, 19–27. https://doi.org/10.1029/2018GL081129

Ergun, R. E., Ray, L., Delamere, P. A., Bagenal, F., Dols, V., & Su, Y. J. (2009). Generation of parallel electric fields in the Jupiter-Io torus wake region. *Journal of Geophysical Research*, *114*, A05201. https://doi.org/10.1029/2008JA013968

Gershman, D. J., Connerney, J. E. P., Kotsiaros, S., DiBraccio, G. A., Martos, Y. M., Viñas, A. F., et al. (2019). Alfvénic fluctuations associated with Jupiter's auroral emissions. *Geophysical Research Letters*, *46*, 7157–7165. https://doi.org/10.1029/2019GL082951

Goertz, C. (1980). Io's interaction with the plasma torus. *Journal of Geophysical Research*, *85*(A6), 2949–2956. https://doi.org/10.1029/JA085iA06p02949

Grodent, D. (2015). A brief review of ultraviolet auroral emissions on giant planets. *Space Science Reviews*, *187*(1-4), 23–50. https://doi.org/10.1007/s11214-014-0052-8

Gurnett, D. A., & Goertz, C. K. (1981). Multiple Alfven wave reflections excited by Io: Origin of the Jovian decametric arcs. *Journal of Geophysical Research*, *86*(A2), 717. https://doi.org/10.1029/JA086ia02p00717

Hess, S. L. G., Bonfond, B., Chantry, V., Gérard, J.-C., Grodent, D., Jacobsen, S., & Radioti, A. (2013). Evolution of the Io footprint brightness II: Modeling. *Planetary and Space Science*, *88*(C), 76–85. https://doi.org/10.1016/j.pss.2013.08.005

Hess, S. L. G., Delamere, P. A., Dols, V., Bonfond, B., & Swift, D. (2010). Power transmission and particle acceleration along the Io flux tube. *Journal of Geophysical Research*, *115*, A06205. https://doi.org/10.1029/2009JA014928

Hess, S. L. G., Zarka, P., Mottez, F., & Ryabov, V. B. (2009). Electric potential jumps in the Io-Jupiter flux tube. *Planetary and Space Science*, *57*(1), 23–33. https://doi.org/10.1016/j.pss.2008.10.006

Hill, T. W., & Vasyliunas, V. M. (2002). Jovian auroral signature of Io's corotational wake. *Journal of Geophysical Research*, *107*(A12), 1464 https://doi.org/10.1029/2002JA009514

Hinton, P. C., Bagenal, F., & Bonfond, B. (2019). Alfvén wave propagation in the Io plasma torus. *Geophysical Research Letters*, *46*, 1242–1249. https://doi.org/10.1029/2018GL081472

Hue, V., Greathouse, T. K., Bonfond, B., Saur, J., Gladstone, G. R., Roth, L., et al. (2019). Juno-UVS observation of the Io footprint during solar eclipse. *Journal of Geophysical Research: Space Physics*, *124*, 5184–5199. https://doi.org/10.1029/2018JA026431

Ingersoll, A. P., Vasavada, A. R., Little, B., Anger, C. D., Bolton, S. J., Alexander, C., et al. (1998). Imaging Jupiter's aurora at visible wavelengths. *Icarus*, *135*(1), 251–264. https://doi.org/10.1006/icar.1998.5971

Jacobsen, S., Neubauer, F. M., Saur, J., & Schilling, N. (2007). Io's nonlinear MHD-wave field in the heterogeneous Jovian magnetosphere. *Geophysical Research Letters*, *34*, L10202. https://doi.org/10.1029/2006GL029187

Jacobsen, S., Saur, J., Neubauer, F. M., Bonfond, B., Gérard, J.-C., & Grodent, D. (2010). Location and spatial shape of electron beams in Io's wake. *Journal of Geophysical Research*, *115*, A04205. https://doi.org/10.1029/2009JA014753

Jones, S. T., & Su, Y.-J. (2008). Role of dispersive Alfvén waves in generating parallel electric fields along the Io-Jupiter fluxtube. *Journal of Geophysical Research*, *113*, A12205. https://doi.org/10.1029/2008JA013512

Lysak, R. L., & Lotko, W. (1996). On the kinetic dispersion relation for shear Alfvén waves. *Journal of Geophysical Research*, *101*(A3), 5085–5094. https://doi.org/10.1029/95JA03712

Louis, C. K., Lamy, L., Zarka, P., Cecconi, B., Imai, M., Kurth, W. S., et al. (2017). Io-Jupiter decametric arcs observed by Juno/waves compared to ExPRES simulations. *Geophysical Research Letters*, *44*, 9225–9232. https://doi.org/10.1002/2017GL073036

Louis, C. K., Prangé, R., Lamy, L., Zarka, P., Imai, M., Kurth, W. S., & Connerney, J. E. P. (2019). Jovian Auroral radio sources detected in situ by Juno/waves: Comparisons with model auroral ovals and simultaneous HST FUV images. *Geophysical Research Letters*, *46*, 11,606–11,614. https://doi.org/10.1029/2019GL084799

Markwardt, C. B. (2009). *Non-linear least-squares fitting in IDL with MPFIT* (Vol. 411, p. 251). Paper presented at Astronomical Data Analysis Software and Systems XVIII, ASP Conference Series.

Matsuda, K., Terada, N., Katoh, Y., & Misawa, H. (2012). A simulation study of the current-voltage relationship of the Io tail aurora. *Journal of Geophysical Research*, *117*, A10214. https://doi.org/10.1029/2012JA017790

Mauk, B. H., Haggerty, D. K., Paranicas, C., Clark, G., Kollmann, P., Rymer, A. M., et al. (2017). Juno observations of energetic charged particles over Jupiter's polar regions: Analysis of monodirectional and bidirectional electron beams. *Geophysical Research Letters*, *44*, 4410–4418. https://doi.org/10.1002/2016GL072286

McComas, D. J., Alexander, N., Allegrini, F., Bagenal, F., Beebe, C., Clark, G., et al. (2017). The Jovian auroral distributions experiment (JADE) on the Juno mission to Jupiter. *Space Science Review*, *213*(1–4), 547–643. https://doi.org/10.1007/s11214-013-9990-9

Mura, A., Adriani, A., Connerney, J. E. P., Bolton, S., Altieri, F., Bagenal, F., et al. (2018). Juno observations of spot structures and a split tail in Io-induced aurorae on Jupiter. *Science*, *361*(6404), 774–777. https://doi.org/10.1126/science.aat1450

Nénon, Q., Sicard, A., Kollmann, P., Garrett, H. B., Sauer, S. P. A., & Paranicas, C. P. (2018). A physical model of the proton radiation belts of Jupiter inside Europa's orbit. *Journal of Geophysical Research: Space Physics*, *123*, 3512–3532. https://doi.org/10.1029/2018JA025216

Neubauer, F. M. (1980). Nonlinear standing Alfvén wave current system at Io: Theory. *Journal of Geophysical Research*, *85*(A3), 1171–1178. https://doi.org/10.1029/JA085ia03p01171

Paranicas, C., Mauk, B. H., Haggerty, D. K., Clark, G., Kollmann, P., Rymer, A. M., et al. (2019). Io's effect on energetic charged particles as seen in Juno data. *Geophysical Research Letters*, *46*, 13,615–13,620. https://doi.org/10.1029/2019GL085393

Pryor, W. R., Rymer, A. M., Mitchell, D. G., Hill, T. W., Young, D. T., Saur, J., et al. (2011). The auroral footprint of Enceladus on Saturn. *Nature Publishing Group*, *472*(7343), 331–333. https://doi.org/10.1038/nature09928

Radioti, A., Lystrup, M., Bonfond, B., Grodent, D., & Gérard, J.-C. (2013). Jupiter's aurora in ultraviolet and infrared: Simultaneous observations with the Hubble Space Telescope and the NASA infrared telescope facility, *Journal of Geophysical Research: Space Physics*, *118*, 2286–2295. https://doi.org/10.1002/jgra.50245

Saur, J., Grambusch, T., Duling, S., Neubauer, F. M., & Simon, S. (2013). Magnetic energy fluxes in sub-Alfvénic planet star and moon planet interactions. *Astronomy and Astrophysics*, *552*, A119. https://doi.org/10.1051/0004-6361/201118179

Saur, J., Janser, S., Schreiner, A., Clark, G., Mauk, B. H., Kollmann, P., et al. (2018). Wave-particle interaction of Alfvén waves in Jupiter's magnetosphere: Auroral and magnetospheric particle acceleration. *Journal of Geophysical Research: Space Physics*, *123*, 9560–9573. https://doi.org/10.1029/2018JA025948

Saur, J., Neubauer, F. M., Connerney, J. E. P., Zarka, P., & Kivelson, M. G. (2004). Plasma interaction of Io with its plasma torus. *Jupiter: The Planet, Satellites and Magnetosphere*, *1*, 537–560.

Su, Y.-J., Ergun, R. E., Bagenal, F., & Delamere, P. A. (2003). Io-related Jovian auroral arcs: Modeling parallel electric fields. *Journal of Geophysical Research*, *108*(A2), 151–111. https://doi.org/10.1029/2002JA009247

Sulaiman, A. H., Hospodarsky, G. B., Elliott, S. S., Kurth, W. S., Gurnett, D. A., Imai, M., et al. (2020). Wave-particle interactions associated with Io's auroral footprint: Evidence of Alfvén, ion cyclotron, and whistler modes, *Geophysical Reasearch Letters*, *47*, e2020GL088432. https://doi.org/10.1029/2020GL088432

Sulaiman, A. H., Kurth, W. S., Hospodarsky, G. B., Averkamp, T. F., Ye, S. Y., Menietti, J. D., et al. (2018). Enceladus auroral hiss emissions during Cassini's grand finale. *Geophysical Research Letters*, *45*, 7347–7353. https://doi.org/10.1029/2018GL078130

Szalay, J. R., Allegrini, F., Bagenal, F., Bolton, S., Clark, G., Connerney, J. E. P., et al. (2017). Plasma measurements in the Jovian polar region with Juno/JADE. *Geophysical Research Letters*, *44*, 7122–7130. https://doi.org/10.1002/2017GL072837

Szalay, J. R., Allegrini, F., Bagenal, F., Bolton, S. J., Bonfond, B., Clark, G., et al. (2020). Alfvénic acceleration sustains Ganymede's footprint tail aurora. *Geophysical Research Letters*, *47*, e2019GL086527). https://doi.org/10.1029/2019GL086527

Szalay, J. R., Bagenal, F., Allegrini, F., Bonfond, B., Clark, G., Connerney, J. E. P., et al. (2020). Proton acceleration by Io's Alfvénic interaction. *Journal of Geophysical Research: Space Physics*, *125*, e2019JA027314. https://doi.org/10.1029/2019JA027314

Szalay, J. R., Bonfond, B., Allegrini, F., Bagenal, F., Bolton, S., Clark, G., et al. (2018). In situ observations connected to the Io footprint tail aurora. *Journal of Geophysical Research: Planets*, *123*, 3061–3077. https://doi.org/10.1029/2018JE005752

Valek, P. W., Allegrini, F., Bagenal, F., Bolton, S. J., Connerney, J. E. P., Ebert, R. W., et al. (2019). Jovian high-latitude ionospheric ions: Juno in situ observations. *Geophysical Research Letters*, *46*, 8663–8670. https://doi.org/10.1029/2019GL084146

Warwick, J. W., Pearce, J. B., Riddle, A. C., Alexander, J. K., Desch, M. D., Kaiser, M. L., et al. (1979). Voyager 1 planetary radio astronomy observations near Jupiter. *Science*, *204*(4396), 995–998. https://doi.org/10.1126/science.204.4396.995

Watt, C. E. J., & Rankin, R. (2007). Electron acceleration due to inertial Alfvén waves in a non-Maxwellian plasma. *Journal of Geophysical Research*, *112*, A04214. https://doi.org/10.1029/2006JA011907

Watt, C. E. J., & Rankin, R. (2012). Alfvén wave acceleration of auroral electrons in warm magnetospheric plasma, in auroral phenomenology and magnetospheric processes: Earth and other planets. *Geophysical Monograph Series*, *197*.

Zarka, P. (1998). Auroral radio emissions at the outer planets: Observations and theories. *Journal of Geophysical Research*, *103*(E9), 20,159–20,194. https://doi.org/10.1029/98JE01323

Zarka, P. (2007). Plasma interactions of exoplanets with their parent star and associated radio emissions. *Planetary and Space Science*, *55*(5), 598–617. https://doi.org/10.1016/j.pss.2006.05.045

Zarka, P., Marques, M. S., Louis, C., Ryabov, V. B., Lamy, L., Echer, E., & Cecconi, B. (2018). Jupiter radio emission induced by Ganymede and consequences for the radio detection of exoplanets. *Astronomy and Astrophysics*, *618*, A84–A89. https://doi.org/10.1051/0004-6361/201833586